Supporting Information

for "Quantifying Signal Dispersion in a Hybrid Ice Core Melting System"

Daniel J. Breton,* Bess G. Koffman,* Andrei V. Kurbatov, Karl J. Kreutz, and Gordon S. Hamilton

E-mail: daniel.j.breton@dartmouth.edu; bess.koffman@maine.edu

CMHS Equipment Details

The Melt Monitor uses a Rabbit Semiconductor (Davis, CA) RCM3700 microcontroller, providing multiple serial communications ports and many digital input/output pins. The temperature controller is an RS-232 enabled Omega Engineering (Stamford, CT) CSC32 communicating with the Melt Monitor via a ModBus interface. The peristaltic pumps (Gilson (Middleton, WI) Minipuls3) and fraction collectors (Gilson model 204) are controlled by the Monitor via a Gilson 508 RS-232→GSIOC interface module. The debubbler optical level sensors and the rotary encoder communicate with the Monitor via digital signals. Due to their high data rate, the electrolytic conductivity meter (Amber Scientific (Ashland, OR) Model 3084) and particle size detector (Markus Klotz GmbH (Bad Liebenzell, Germany) Abakus) instruments communicate directly with the PC.

Rotary encoder melt displacement system

Melt displacement of the ice core is determined by a CUI (Tualatin, OR) AMT-103V rotary encoder which measures the angular displacement θ of a cogged pulley in the weight/counter-weight

*To whom correspondence should be addressed

system shown in Figure 1 of the main paper. Calibration of the system is performed by moving the weight through a known distance z and using this distance to calculate an effective pulley diameter $D_{\text{eff}} = 2z/\theta$ where θ has units of radians. For our encoder setup, D_{eff} =2.584 cm and, coupled with the 11-bit encoder resolution (2048 pulses per rev), the vertical resolution for melt displacement is $\pm$0.04 mm.

Parcel Tracking Example

The parcel generation interval (1 parcel mm^{-1} of melt displacement) is chosen such that the parcel transit time for a CFA instrument is greater than or equal to the instrument measurement interval. If the parcel transit time was less than the measurement interval, the ECM data would be missing some depths and the PSD data would indicate the sum of several parcels, thus degrading the maximum possible vertical resolution for the CFA system.

The highest measurement frequency for both CFA instruments is 1 Hz. For steady state melting (i.e. equal parcel birth and termination rates) this also represents the upper limit for parcel generation rate. The melt speed to achieve this resolution-limiting parcel generation rate (using a parcel birth interval of 1 mm) is 60 mm/min, well above the typical 15 to 30 mm/min melt speeds observed for this melting system. Thus our CFA measurements usually contain 2-4 data points on each parcel as they traverse the sensor volume. The multiple data points for each parcel are then post-processed (averaged for ECM data and summed for PSD data) to produce single-valued records for a given depth.

Figure S1 represents a simple composite tubing system in both real and volume space. Λ's for both instruments and parcels could also be determined using a volumetric flow meter, rather than depending on pump constant measurements for flow rate determination. However, this approach cannot be used in series with sample destined for ICP-SMS analysis due to the extraordinary sensitivity of this measurement to contamination from the flow meter.

Figure S2 gives a short example of the parcel tracking algorithm in action.

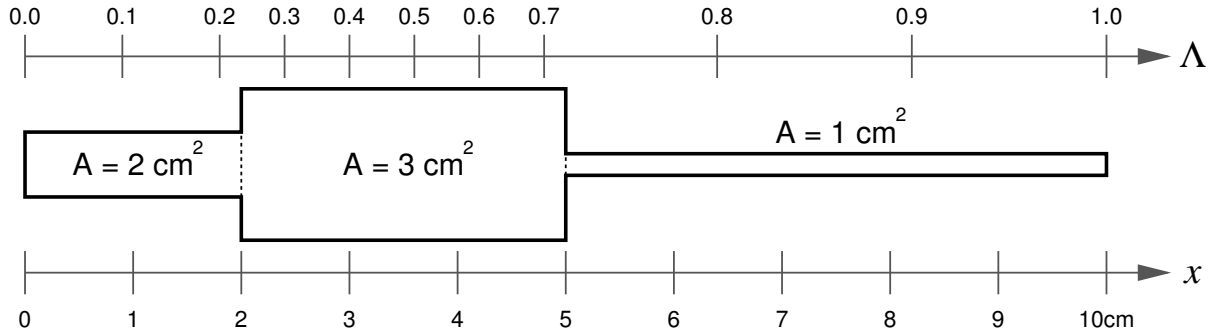

Figure S1: Example composite tubing built from 3 sections with different cross-sectional areas A. Relative position Λ scale and actual position x scale shown to illustrate the relationship between actual and volume space representations of the composite tubing length.

Parcel Number	82	81	80	79	78	77	76	75	74	73
Parcel Λ−value	0.0 MH	0.22	0.35	0.42	0.50 PSD	0.63 ECM	0.69	0.81	0.88	1.00 VIAL
Array Index	0	1	2	3	4	5	6	7	8	9

(a)

Parcel Number	90	89	88	87	86	85	84	83	82	81	80	79
Parcel Λ−value	0.0 MH	0.18	0.29	0.37	0.48	0.53 PSD	0.59	0.67 ECM	0.72	0.86	0.94	1.00 VIAL
Array Index	0	1	2	3	4	5	6	7	8	9	10	11

(b)

Figure S2: Example of parcel tracking algorithm for a very small sample handling system. For this example, $\Lambda_{PSD} = 0.50$, $\Lambda_{ECM} = 0.60$ and $\Lambda_{vial} = 1.0$. In (a), the encoder has just registered the 82nd mm of melt displacement on this core and therefore parcel 82 has just been born. Older parcels have traveled farther; parcel 78 has just reached the ECM while parcel 73 is currently filling a vial. After 8 more mm of melt displacement, we have the case shown in (b). Parcel 90 was just born, 82 has passed through both CFA instruments and 79 is filling a vial. The number of live parcels has increased (perhaps due to higher melt speed) since 8 parcels were born, but only 6 have been terminated in the interval between (a) & (b).

Parcel Tracking of Air/Water Mixtures

In the CMHS system, we run two parcel tracking legs, coupled at the debubbler: one for the air/water mixture present in the meltwater supply system (melthead $\rightarrow$ debubbler) and another for the solid water system (debubbler $\rightarrow$ vial). Because the air/water mixture volume is larger than the solid water volume, the meltwater flow rate is $(\rho_{\text{water}}/\rho_{\text{core}})$ times faster than the solid water flow rate leaving the debubbler.

A major assumption in the meltwater parcel tracking calculation is that a peristaltic pump moves air and water with equal effectiveness ($K_{\text{air}} = K_{\text{water}}$). We have tested this assumption in the laboratory and found it to be true within the uncertainty ($\pm 5\%$) of the measurement. Therefore, in the meltwater supply system, parcels *regardless of their air/water composition* are transported the same relative distance per pump revolution.

Upon arrival at the debubbler, the parcel is transferred to the solid water parcel tracking system. The volume change due to de-bubbling makes no difference to the parcel tracking algorithm because all parcels start at the same point (debubbler), are transported the same relative distance per pump revolution, and end at the same point (vial).

Loss-Free Debubbler Details

Our debubbler is a simple two-part design which easily can be disassembled and cleaned. The upper section consists of a 2 cm long section of transparent, 7.94 mm OD FEP tubing (Cole-Parmer, Vernon Hills, IL), while the lower section is a custom machined section of PTFE that serves to couple the upper section to a 2.8 mm ID STAPURE tube below.

The level sensing system consists of two Omron (Schaumburg, IL) EE-SX3070 Transmissive Photomicrosensors which send infrared beams ($\sim$870 nm wavelength) across the upper, transparent portion of the debubbler vessel. The path taken by the light beam is affected by the presence or absence of water inside the debubbler vessel, as shown in Figure S3. The path differences are due to refraction: water and FEP share very similar indices of refraction (causing very small angle

refraction) while air has a much smaller index of refraction than either water or FEP (causing larger angle refraction). For the 8.0 mm beam path length of the EE-SX3070, the difference in beam path is small, but reliably detectable with the 0.5 mm collimation slit built into the sensors.

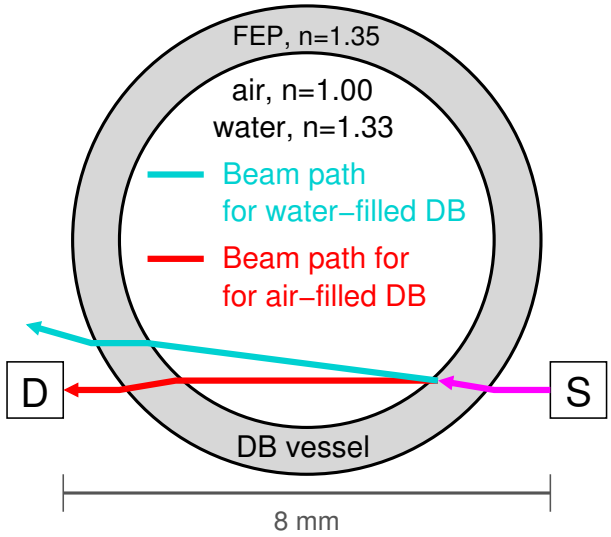

Figure S3: Top down view of debubbler and level sensing system. Beam paths are calculated using geometric optics. S=light source, D=light detector, n=index of refraction. Note that the beam axis is *not* along the debubbler vessel diameter - such a placement would result in the same beam path for both air and water scenarios since no refraction is possible. The detector sends 0V (+5V) to the Melt Monitor for air (water) filled debubbler.

The optical level sensing system (shown in Figure S4) requires good alignment which is achieved by a custom mounting frame and debubbler vessel positioning screws. The entire system is mounted under a Class 100 HEPA filtering hood to avoid particulate contamination.

Because there are only two level sensors, debubbler level is measured by the Melt Monitor to be in one of three states: LOW, NORMAL or HIGH. The Monitor responds by operating the downstream pumps at 0% (for LOW levels), 80% (NORMAL) and 120% (HIGH) of the meltwater supply pump flow rate. Effective level control requires accurate K values for all pumps in the system to be determined and entered into the Monitor before melting.

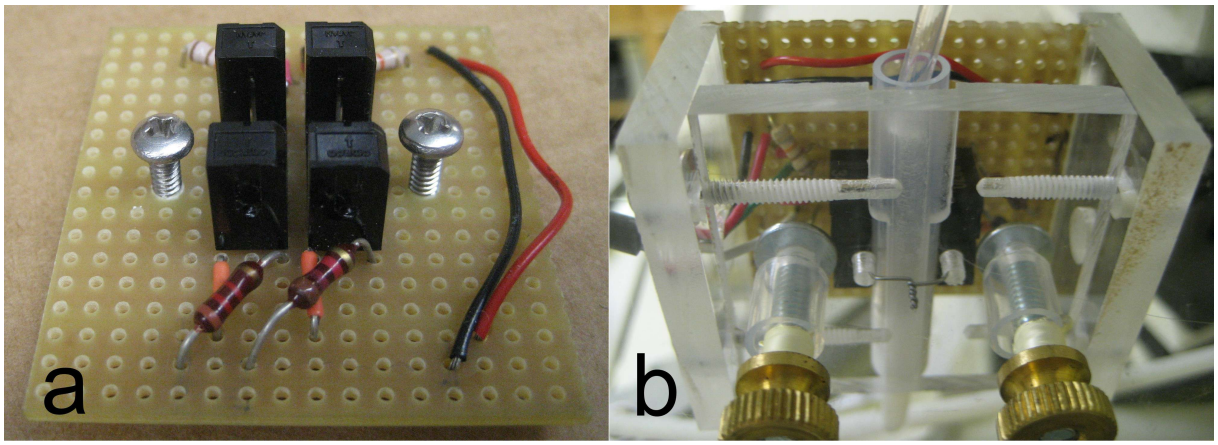

Figure S4: Images of (a) the optical level sensing circuit board with debubbler positioning screws and (b) the full assembly of debubbler vessel, level sensors and mounting frame. Input tubing from supply pump enters from the top, output tubing to dust/geochemistry tee-fitting at bottom.

Glaciochemical Analyses

The primary reason for developing our hybrid ice core melting system was to make parallel analyses of microparticle and trace elemental concentrations with accurate, mm-scale depth co-registration, while preserving the benefits conferred by discrete ICP-SMS analysis (i.e., sufficient acidification time for mineral dissolution, longer scan times, and the ability to collect an archive). Because CFA instrumentation has the potential to contaminate trace element concentrations, we maintained a dedicated trace element sample line in our CMHS system. Table S1 provides major and trace element concentrations measured in deionized water blanks along with detection limits (DL) for the CMHS system and our ICP-SMS. These concentrations compare favorably to those measured using other continuous ice core melter systems (*1*, *2*), and are generally below environmental concentrations measured in Antarctic snow and ice (*3*). Because we used a solid nickel 270 melting disc ($>$ 99.99% Ni), we do not consider measurements of Ni to be reliable.

Table S1: Average instrumental and melter system (CMHS) blanks and instrumental and CMHS detection limits, all in ng L^{-1}.

Analyte[1]	Inst. blank[2]	Inst. DL[3]	CMHS blank[4]	CMHS DL[5]
^{27}Al(MR)	5.2±2.2	6.8	<CMHS DL	210
^{138}Ba(LR)	<IDL	0.16	<CMHS DL	4.6
^{44}Ca(MR)	140±34	100	280±70	210
^{111}Cd(LR)	0.034±0.011	0.032	<CMHS DL	0.11
^{140}Ce(LR)	0.00506±0.00243	0.00729	<CMHS DL	0.0450
^{59}Co(MR)	0.081±0.043	0.074	0.071±0.036	0.11
^{52}Cr(MR)	0.15±0.041	0.12	<CMHS DL	1.2
^{133}Cs(LR)	0.0042±0.0020	0.0061	0.010±0.0038	0.011
^{63}Cu(MR)	<IDL	2.4	16±5.2	16
^{56}Fe(MR)	<IDL	9.5	11±4.2	13
^{39}K(HR)	110±47	140	<CMHS DL	410
^{139}La(LR)	0.0221±0.00780	0.0236	<IDL	0.0246
^{7}Li(LR)	0.14±0.024	0.073	<CMHS DL	0.50
^{24}Mg(MR)	82±6.5	20	260±110	320
^{55}Mn(MR)	<IDL	0.45	1.7±0.83	2.5
^{23}Na(MR)	<IDL	270	<CMHS DL	1950
^{208}Pb(LR)	0.067±0.022	0.065	<CMHS DL	1.5
^{141}Pr(LR)	0.00880±0.00150	0.00462	<IDL	0.00487
^{32}S(MR)	130±42	130	<CMHS DL	400
^{88}Sr(LR)	0.16±0.073	0.22	1.9±0.77	2.3
^{47}Ti(MR)	0.39±0.16	0.50	<CMHS DL	4.1
^{238}U(LR)	0.00570±0.00190	0.00560	0.00498±0.00246	0.00738
^{51}V(MR)	0.092±0.031	0.093	<CMHS DL	0.64
^{66}Zn(MR)	<IDL	6.1	<CMHS DL	49

[1]LR indicates low resolution mode ($m/\Delta m = 300$) and MR indicates medium resolution mode ($m/\Delta m = 4000$) for the ICP-SMS. [2]Mean of 10 deionized water blanks. [3]Instrumental detection limit calculated as 3σ of 10 water blanks. [4]Mean of 10 deionized water blanks sent through the entire CMHS system and collected via fraction collector. [5]CMHS detection limit calculated as 3σ of 10 water blanks sent through the CMHS system.

Uncertainties

Pump Constants

Pump constant data collection was required at the start of each melting day because K is slightly different each time the sample tubing is clamped into the pump. A stable pump constant can be achieved by running the clamped tubing through approximately 50 rev before taking K data. We chose thick walled, 1.6 mm ID STAPURE tubing (STA-PURE, Gore and Associates, Elkton, MD) which provided stable ($\pm$ 0.5%) pump constants, excellent longevity and cleanliness for trace metal analysis.

The uncertainty in K can be determined by

$$(\Delta K)^2 = \left(\frac{\partial K}{\partial V}\right)^2 (\Delta V)^2 + \left(\frac{\partial K}{\partial R}\right)^2 (\Delta R)^2$$

which evaluates to

$$(\Delta K)^2 = \left(\frac{1}{R^2}\right) (\Delta V)^2 + \left(\frac{V^2}{R^4}\right) (\Delta R)^2.$$

For the CMHS system, $\Delta V = 0.002$ mL and $\Delta R = 0.1$ rev. Using these uncertainties with typical pump calibration values of $V = 13.14$ mL in $R = 57.2$ rev, we calculate $K = 0.2296 \pm 0.0004$ mL/rev, or about 0.2%. Measuring K over larger numbers of pump revolutions reduces the uncertainty in the value. A typical 100 cm ice core produces 140 mL of inner channel meltwater, requiring roughly 600 pump revolutions. The above quoted ΔK results in a volume uncertainty of 0.56 mL (0.4% of 140 mL) after 600 rev.

Parcel Location

The uncertainty in the location of parcel i can be calculated from

$$(\Delta \Lambda_i)^2 = \left(\frac{\partial \Lambda_i}{\partial R_i}\right)^2 (\Delta R_i)^2 + \left(\frac{\partial \Lambda_i}{\partial R_{\text{sys}}}\right)^2 (\Delta R_{\text{sys}})^2$$

which evaluates to

$$(\Delta\Lambda_i)^2 = \left(\frac{1}{R_{\text{sys}}}\right)^2 (\Delta R_i)^2 + \left(\frac{R_i}{R_{\text{sys}}^2}\right)^2 (\Delta R_{\text{sys}})^2$$

Dispersion Effects on Resolution

Depth resolution in CFA systems is generally dispersion-limited, meaning that the system RTD effectively quantifies the resolution. Figure S5 illustrates the approach to the resolution limit for our system, using the actual system RTD and unit delta function input events with event separation $\Delta z = 8$, 9 and 10 mm. The first two input pairs ($\Delta z = 8$ and 9 mm) are unresolvable by our system using the 10% valley criterion. The final pair ($\Delta z = 10$ mm) slightly exceeds the criterion; however, we report a 10 mm depth resolution to ensure our stated value is conservative.

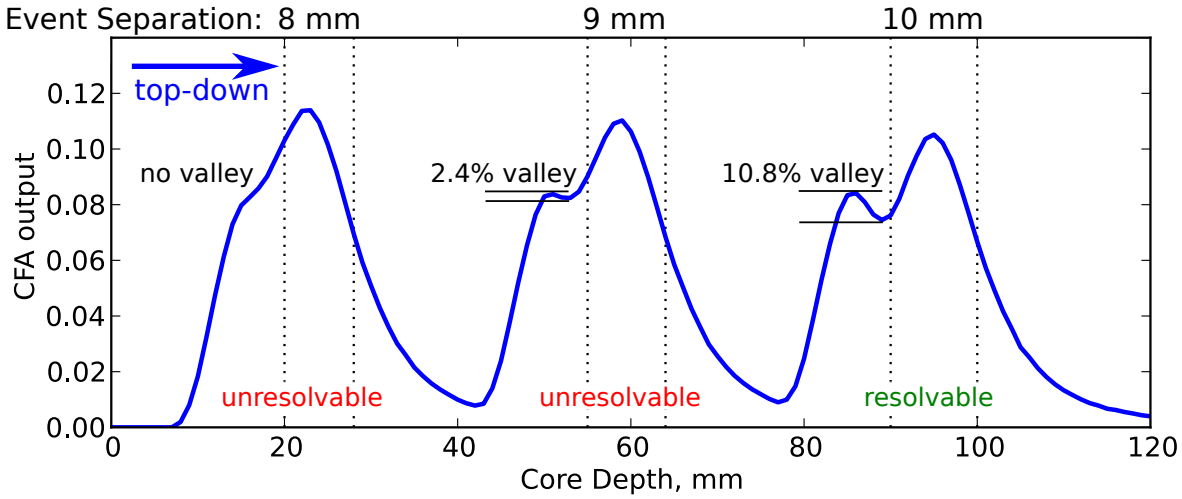

Figure S5: Approach to the resolution limit for the CMHS system. Depths of unit-magnitude delta function inputs in the core (917 kg m^{-3}) are indicated by dashed vertical lines at 20, 28, 55, 64, 90 and 100 mm.

References

(1) Osterberg, E. C.; Handley, M. J.; Sneed, S. B.; Mayewski, P. A.; Kreutz, K. J. Continuous Ice Core Melter System with Discrete Sampling for Major Ion, Trace Element, and Stable Isotope Analyses. *Environmental Science & Technology* **2006**, *40*, 3355–3361, PMID: 16749705.

(2) Knusel, S.; Piguet, D. E.; Schwikowski, M.; Gaggeler, H. W. Accuracy of Continuous Ice-Core Trace-Element Analysis by Inductively Coupled Plasma Sector Field Mass Spectrometry. *Environmental Science & Technology* **2003**, *37*, 2267–2273, PMID: 12785535.

(3) Dixon, D.; Mayewski, P.; Korotkikh, E.; Sneed, S.; Handley, M.; Introne, D.; Scambos, T. A spatial framework for assessing current conditions and monitoring future change in the chemistry of the Antarctic atmosphere. *Cryosphere Discussions* **2011**, *5*, 885.